Vacuum 144 (2017) 217–228

Contents lists available at ScienceDirect

Vacuum

journal homepage: www.elsevier.com/locate/vacuum

Characterisation of Cu_2O, Cu_4O_3, and CuO mixed phase thin films produced by microwave-activated reactive sputtering

Yahya Alajlani [a, b, *], Frank Placido [a], Anders Barlow [c], Hin On Chu [a], Shigeng Song [a], Saeed Ur Rahman [a], Robert De Bold [d], Des Gibson [a]

[a] Scottish Universities Physics Alliance (SUPA), Institute of Thin Films, Sensors and Imaging, University of the West of Scotland, Paisley, UK
[b] Department of Physics, Faculty of Science, Jazan University, Jazan, Saudi Arabia
[c] Centre for Materials and Surface Sciences (CMSS), Department of Chemistry and Physics, La Trobe University, Melbourne, Victoria, Australia
[d] Institute for Infrastructure and Environment, School of Engineering, University of Edinburgh, Edinburgh, UK

ARTICLE INFO

Article history:
Received 23 March 2017
Received in revised form
2 August 2017
Accepted 5 August 2017
Available online 7 August 2017

Keywords:
Nanostructure
Copper oxide
Microwave-activated reactive sputtering
OJL model

ABSTRACT

Copper readily forms three oxides, CuO, Cu_4O_3 and Cu_2O, widely recognised as the most promising p-type oxides because of their desirable optical and electrical properties and potential use in solar cells, transparent electronics as well as other specialised applications such as electrodes for rechargeable lithium batteries, catalysis and memristors. For large-scale implementation of devices, magnetron sputtering is a practical method of producing metal oxides; however, sputtered copper oxides tend to form as a mixture of the oxides, with Cu_2O being particularly difficult to produce reliably in pure form. Here, nanostructured thin films of copper oxides were prepared by a variation on reactive sputtering known as microwave-activated reactive sputtering under various rates of oxygen flow. Microwave-activated reactive sputtering was shown to be a suitable technique for the inexpensive production of large areas of copper oxide thin films at near room temperature, facilitating deposition on a wide variety of substrates including polymers. Furthermore, it was demonstrated that the sputtered films develop through CuO, Cu4O3 and Cu2O mixed phases as oxygen flow rate is increased. The preparation of a given stoichiometry for a particular application can be achieved by varying the flow rate of oxygen during the microwave-activated reactive sputtering process.

1. Introduction

The facile and inexpensive production of large areas of copper oxide thin films is desirable because of the very many potential applications. For example, it has been noted that the development of new applications of transparent electronics such as displays and solar cells with improved efficiency and reduced costs requires inexpensive materials for both n-type and p-type semiconductors along with lower energy production methods [1,2]. One of the main factors for the optimal use of copper oxides in particular applications is the control of the deposition process [3].

Cuprous oxide (Cu_2O) and cupric oxide (CuO), are attractive material choices for transparent electronics because copper is an inexpensive and abundant metal, and the oxides are natural p-type semiconductors with a direct band gap [4–6]. Both oxides may be useful for solar cells, although CuO has higher absorbance over a wider wavelength range than Cu_2O. On the other hand, for transparent electronics Cu_2O has the advantage of greater transparency in the visible spectrum. The two oxides have distinctly different properties, with Cu_2O being a yellow/red colour and CuO being a much darker brown/black colour in thin film form due to differences in the band gap and dispersion of the extinction coefficient over the visible/near infrared region of the spectrum [7]. Bandgaps in the range of 2.0–2.6 eV have been reported for Cu_2O films [8], while nominally CuO films are typically in the lower range of 1.2–1.6 eV [9]. The rather wide ranges reported for material and electrical properties reflect the fact that films produced by many of the proposed fabrication methods invariably contain varying mixtures of copper and copper oxide phases and are rarely pure forms of the oxides. This was demonstrated by Drobny & Pulfrey [10], who found that reactive sputtering of copper oxide at higher oxygen partial pressures deposited more oxygen rich phases: Cu_2O + Cu at

* Corresponding author. Scottish Universities Physics Alliance (SUPA), Institute of Thin Films, Sensors and Imaging, University of the West of Scotland, Paisley, UK.
E-mail address: yaaa08@gmail.com (Y. Alajlani).

http://dx.doi.org/10.1016/j.vacuum.2017.08.005
0042-207X/

lower partial pressures, then Cu_2O only, then $Cu_2O + CuO$, and then finally CuO only at higher partial pressures.

However, since the early 2000s, it has been recognised that sputtering can in fact result in three oxides, with Cu_4O_3 being readily formed in addition to CuO and Cu_2O and many earlier papers have failed to recognise this fact [11,12]. Cu_4O_3, known as paramelaconite in mineral form, is itself an interesting material, with potential use in catalysis [13–15].

Ogwu et al. [16], found that the sheet resistance of copper oxide thin films prepared by reactive magnetron sputtering increased with increased O_2 flow rates during production. Therefore, it can be assumed that the presence of the more oxygen rich phases of copper oxide result in greater resistivity. Another very promising application area, for Cu_2O thin films, is in memristors [17], the fourth passive circuit element (after resistors, capacitors and inductors) [18].

For the case of solar cells, it is usual to combine copper oxides with an n-type semiconductor film such as ZnO to fabricate p-n heterojunctions [19,20]. Solar cells produced from copper oxide thin film have a theoretical efficiency of approximately 20% [21,22]; however, the best achieved efficiency so far is 6% [23].

There are numerous methods to produce copper oxide thin films, such as thermal oxidation [24], electrodeposition [9], chemical brightening [25], spraying [8], chemical vapour deposition [26], plasma evaporation [8], vacuum evaporation [27], molecular beam epitaxy [28], reactive sputtering [9,10,25]. All noted methods produce a mixture of phases of Cu, CuO, and Cu_2O [29]. Balamurugan and Mehta [8] used the activated reactive evaporation technique and varied the nanocrystalline structure by varying the deposition parameters. The crystallinity was then analysed by x-ray diffractometer (XRD). The results showed that a single phase of Cu_2O could be deposited at relatively low substrate temperatures using this technique.

Papadimitropoulos et al. [27] grew copper oxide layers by vacuum evaporation of copper onto silicon substrates in a nitrogen-oxygen atmosphere at temperatures between 185C and 450C. The Tauc-Lorentz model was successfully used to extract the refractive indices of the films. Li et al. (2011) used a variation of sputtering known as HITUS and showed that single phase Cu_2O could only be prepared within a very narrow range of deposition parameters.

The consensus of previous work is that copper oxides are potentially very useful materials but are particularly difficult to grow as a pure phase, free of contamination from other phases. While oxygen flow rate is the most important parameter, it appears that other process parameters also need careful control. This suggests that commercial applications requiring pure phases to be deposited reproducibly on large areas may be difficult to achieve, especially when cost and substrate factors require room temperature deposition without further processing steps such as annealing.

This paper focuses on a scalable deposition method with proven commercial success, although not yet in widespread use, known as microwave-activated reactive sputtering (MARS). This method uses a pulsed DC power supply for sputtering plus a separate microwave source in a rotating drum configuration to achieve large area, room temperature deposition of a wide variety of metal oxides, nitrides and oxynitrides [30,31]. Excellent control of deposition parameters allows deposition of high performance optical filters [32], including rugate-type filters, which require thick films to be grown with continuously variable refractive index [33,34]. Other advantages of this type of sputtering are that materials with very high melting points can be sputtered easily [35], whereas techniques such as evaporation can be difficult or impossible. Sputtered films usually have better substrate adhesion than evaporated films. Sputtering can also be undertaken at low temperatures in order to avoid damage to the substrate or other layers. Given that a target can be composed of a large amount of material and is maintenance free, the technique is well-suited for ultrahigh vacuum applications.

In this paper copper oxide films have been grown by MARS. With these films of 500 nm thickness it has not been possible to obtain quantitative compositional information with the techniques available but qualitative results from optical spectroscopy, XRD, Raman and XPS are presented in some detail. It is demonstrated that the sputtered films develop through CuO, Cu_4O_3 and Cu_2O mixed phases as oxygen flow rate is increased and can be successfully and reproducibly grown at room temperature. A pure form of Cu_2O is only produced in a very narrow range of oxygen flow.

2. Experimental procedures

In this work, a MARS system (MicroDyn® 40,000) equipped with a 127 mm × 380 mm high-purity copper target (>99.99%), 10 kW DC power supply (Advanced Energy MDX 10 with Spark-le V arc controller) and a 3 kW plasma source was used. This is a turbo-pumped system with an added Polycold 330 water trap and is capable of reaching an operating pressure of ~10^{-6} torr in 15 min. The rotating drum in this model rotates about a horizontal axis at 60 revs/min and is capable of holding over 3600 cm^2 of substrates. Mass flow controllers were used to control the flow rates of the gases, argon, and oxygen. Argon is admitted at the target position and oxygen at the microwave position. The separate microwave source offers several advantages in this system. Substrates passing the target receive a coating of a few nanometres of predominantly metal, which is then oxidized in the region of the microwave plasma, which is rich in atomic oxygen. The separation of deposition and oxidation greatly reduces the potential for poisoning of the target and arcing. The atomic oxygen is around 10 times more reactive than molecular oxygen and so uses lower oxygen flow rates, in addition the microwave plasma acts as a virtual anode, reducing the disappearing anode effect.

Here we use 30 mm by 12 mm by 1 mm thick glass substrates (standard microscope slides) and 20 mm diameter by 2 mm thickness circular silica substrates cleaned using an ultrasonic system (Optimal UCS40). Several experiments were undertaken where thin films were deposited on the substrates under conditions where the oxygen flow was varied from 10sccm to 28sccm. In all cases reported here, the argon flow rate was constant at 150 sccm. It can be noted that because of the microwave plasma, for reasons outlined above, the oxygen/argon ratios used here are very low compared to those necessary in conventional sputtering, where ratios of up to 0.5 or higher are necessary to produce CuO. The processes were halted once a thickness of 500 nm was achieved, controlled by an Inficon quartz crystal controller (and confirmed later by SEM).

3. Characterisation

Samples were imaged at various magnifications using a Hitachi S4100 field emission scanning electron microscope (SEM). This system has magnification of 40,000 times, a resolution of 1.5 nm, and acceleration voltage for primary electrons of up to 30 kV. The crystalline structure of the thin films was determined by X-ray diffractometry (XRD) (Siemens D5000) with CuK α radiation (40 kV, 30 mA). The diffraction angle was set between 30° and 50° with 1 scan (count) per second at 0.2 increments.

X-ray photoelectron spectroscopy (XPS) was performed on an AXIS Nova (Kratos Analytical, Manchester, UK), utilising a monochromatic AlKα source (1486.6 eV) operated at 225 W (15 kV, 15 mA), and maintaining a base pressure of better than 1×10^{-9} mbar. Analysis area was defined by the spectrometer and chosen to be 400 × 700 μm^2 for all analyses. Survey and high

resolution spectra were collected at pass energy of 160 eV and 20 eV respectively. Charge neutralisation was used throughout the analysis. Three points were analysed on each sample surface.

The transmission and reflection spectra of the thin films, deposited on the silica substrates, were measured using an Aquila Instruments' nkd-8000 spectrometer with Pro-Optix software. Samples were all examined in S-polarized light at 10° angle of incidence, both in transmission and reflection over the 400–1100 nm wavelength range.

Data from each sample was analysed by the W Theiss SCOUT programme using the OJL model, named after O'Leary, Johnson, and Lim [36]. The material composition and transmittance and reflectance spectra were inputted and the programme simulated similar spectra using optical band gap, Eg, damping constant, γ, refractive index, n, extinction coefficient, k, and film thickness as fit parameters. This, in effect, is a method to compute the values of these parameters and the degree of correlation of the simulated spectrum to the analysed spectrum is an indicator of the accuracy of those parameters.

Raman scattering measurements were taken using a Thermo Scientific DXR Raman Microscope. Samples were measured using a 100× objective using 532 nm 1.0 mW laser excitation. Fluorescence corrections and medium cosmic ray thresholds were applied to the data collection.

4. Results and discussion

4.1. SEM analysis

Fig. 1 shows the SEM images of the thin layers deposited under oxygen flows of 10, 14, and 17sccm revealing their thicknesses and smooth surface topography.

4.2. XRD analysis

The XRD results of the samples can be seen in Fig. 2.

The location of the spikes in intensity on the XRD plot at the various 2θ angles of incidence can be related to the material composition and crystalline orientation. The 2θ angle values for each copper composition were taken from JADE5 PDF tables or Blobaum et al. [11] and can be seen in Table 1.

As noted by Blobaum, et at [11], sputtering of copper in a room temperature oxygen environment produces Cu_4O_3 at a similar XRD 2θ angle to CuO (111) sputtered in a heated oxygen environment. Therefore, given the low temperature nature of MARS, it is considered likely that the copper oxide phase present at ~38° is Cu_4O_3 and not CuO. Subsequent Raman analysis confirm this.

Consequently, it can be seen that under the various oxygen flows, the composition and orientation of the crystalline structure of the thin layers varies. Also, from the shape of the peaks from the XRD plot, it can be inferred that those with a sharper peak are more crystalline than those with a broader peak, which are more amorphous.

Fig. 2 shows a change in behaviour as oxygen flow rates increase. At oxygen flow rates between 11sccm and 16sccm, there are always multiple phases present of Cu_2O and Cu_4O_3 present. However, under oxygen flow rates of 17sccm or greater, CuO is the dominant species. It is not surprising that the most oxygen rich phase forms exclusively under the higher oxygen flow rates.

The presence of each phase is noted in Table 2 based on the rate of oxygen flow.

4.3. XPS analysis

X-ray Photoelectron Spectroscopy (XPS) was performed to identify the chemical composition of the copper surfaces. Survey spectra for the 10sccm and 17sccm samples given in Fig. 3a. The only elements detected at the surface were Cu, O and C, where the carbon was assumed to be adventitious contamination. The energy scale was calibrated by setting the carbon peak to 284.8eV. Table 3 presents the results of the quantification of chemical composition based on survey spectra for samples from 10 to 20sccm. Unfortunately, it was not possible to obtain XPS measurements for samples produced under oxygen flow rates of 24, 26, and 28sccm. Upon initial inspection it would appear as though the atomic percentages do not support the presence of the three oxides of copper (Cu_2O, Cu_4O_3 and CuO) observed by XRD earlier since the ratio of Cu to O (Cu:O) is around 1:1 for all samples. However XPS is expected to be far more surface sensitive than XRD, with most of the signal (95%) coming from <8 nm depth from the surface. Thus analysis simply based on atomic percentages is not sufficient in this case as it is influenced by any rearrangement of the surface atoms resulting in the formation of surface oxides. Therefore we turn to analysing the high resolution spectra, and referring to reference data for known copper compounds.

Reference Cu 2p and Cu *LMM* spectra of three copper materials; Cu metal, Cu_2O (Cu^{1+} reference) and CuO (Cu^{2+} reference) were obtained from the Open Access XPS Reference Database XPSSurfA [37] and are reproduced in Fig. 3b. The three materials can be distinguished from one another when both the Cu 2p and Cu *LMM* regions are analysed together. Cu 2p for Cu metal shows a sharp $2p_{3/2}$ peak at 932.4eV, with no satellite features. The Cu^{1+} oxide (Cu_2O) has a similar $2p_{3/2}$ position but also shows a weak satellite feature around 946eV. The Cu^{2+} oxide (CuO) has a shifted peak position of 933.6eV and a strong satellite. The peak positions of the three Cu *LMM* regions show distinct energies of 918.8eV, 916.7eV and 917.7eV for the Cu^0, Cu^{1+} and Cu^{2+} materials respectively. Thus scans of the Cu2p and Cu *LMM* regions were collected on each sample at three points on the surface, and representative spectra are given in Fig. 3c and d for the 10sccm and 17sccm samples. The $Cu2p_{3/2}$ region of the doublet presented with an intense component at binding energy 932.5eV along with a less intense shoulder at 934.4eV. The higher binding energy shoulder was taken to be the Cu^{2+} compound CuO. Present also in the Cu2p region were a set of satellite features from 940 to 947eV. These can be identified as satellite features for the Cu^{1+} and Cu^{2+} oxidation states, and are not present for metallic copper as seen in the reference data and literature [38-40]. Investigation of the Cu *LMM* feature (see Fig. 3d) for these samples shows an intense peak at 916.7eV for 10sccm and 917.4eV for 17sccm, indicative of a greater amount of Cu^{1+} and Cu^{2+} present at each of these surfaces respectively. Thus, the lower binding energy component in the Cu $2p_{3/2}$ region is assumed to be predominantly from Cu^{1+}, and Cu_2O, and two components can be fitted to the Cu $2p_{3/2}$ feature for the Cu^{1+} and Cu^{2+} states.

With increased flow rate the ratio of the Cu^{1+} to Cu^{2+} states could then be monitored via the area of the fitted components, along with the position of the Cu *LMM* peak, as given in Fig. 3e and f. It was observed that at a flow rate of 12–15sccm a shift occurs in the dominant oxidation state detected by XPS, with a sharp rise in ratio of Cu^{2+} occurring beyond this value. This is observed in both the ratio of the fitted components (Fig. 3e) and the position of the *LMM* feature (Fig. 3f). From the analysis of these spectra, and with comparison to the reference data for Cu, Cu_2O and CuO in Fig. 3b, we can conclude the chemical composition of the surfaces to be mostly Cu_2O for ~10–14 SCCM, an intermediate oxide of Cu_4O_3 (a mixture of Cu^{1+} and Cu^{2+}) for ~12–16 SCCM, and CuO for ~14–20 SCCM, and these are labelled in Fig. 3e and f as the dominant compositions. This is in excellent agreement with the XRD results presented earlier.

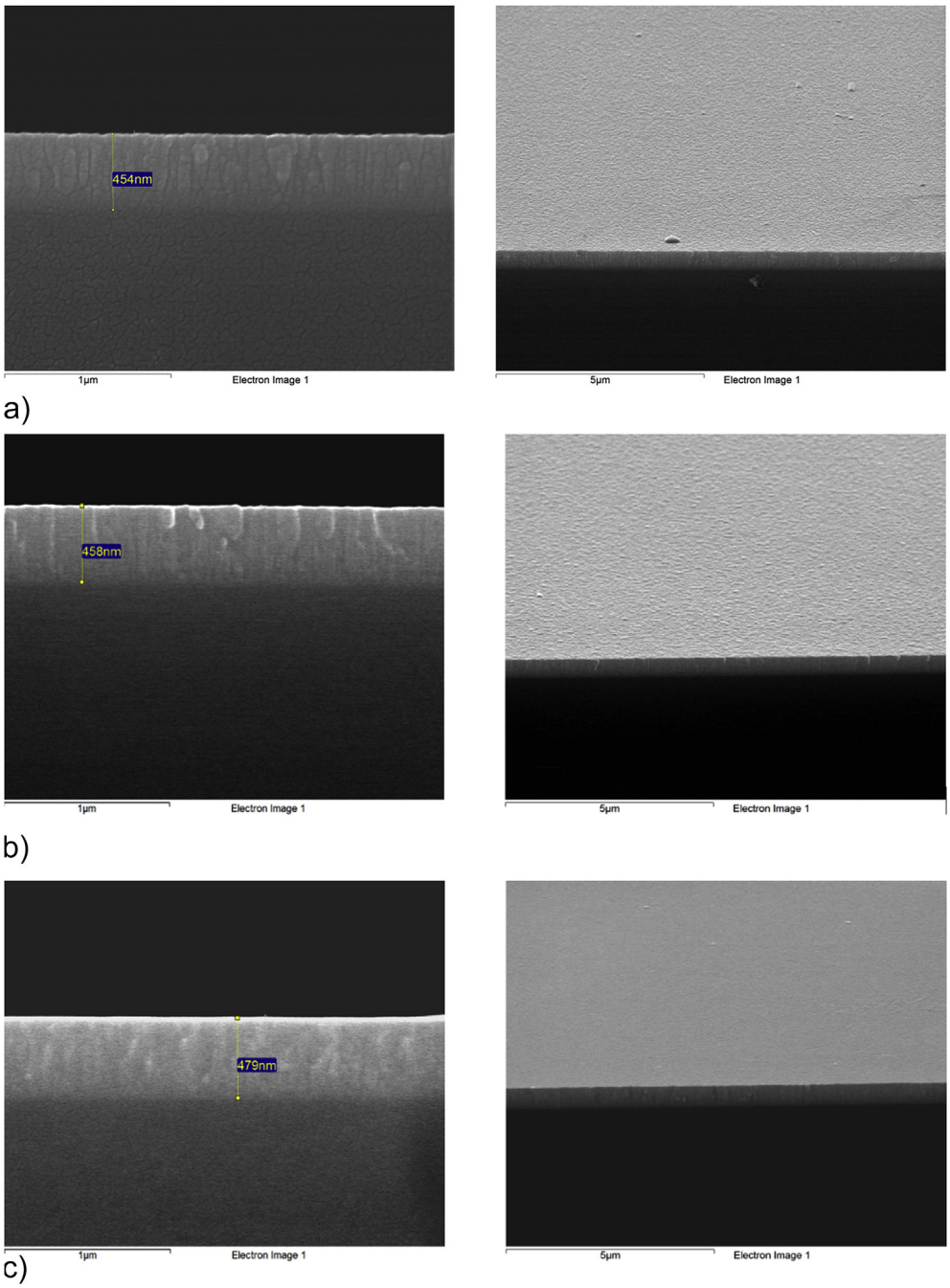

Fig. 1. SEM of samples under various oxygen flow rates.
The SEM images of the thin films confirm the thicknesses and surface topographies.

4.4. Optical spectroscopy

For samples produced under oxygen flows of 10 to 16sccm and 17 to 28sccm, Fig. 4 and Fig. 5, respectively, show the optical properties (transmittance, reflectance and absorptance) of the samples across the visible spectrum (400 nm–1100 nm).

The Aquila instrument directly measures transmittance and reflectance from the same area of the film. The oscillations observed in these spectra are due to coherent interference of the light reflected from the top and bottom surface of the thin films. It is notable, expected from theory, that these oscillations are dampened greatly in the transmittance spectrum as the extinction factor increases, but are still easily observed in the reflectance spectrum. Given the high reflectance, absorptance, A, is calculated using both measured transmittance, T, and reflectance, R, from Eq (1).

$$A = 1 - T - R \quad \begin{matrix} A = \text{absorptance} \\ T = \textit{transmittance} \\ R = \textit{reflectance} \end{matrix} \tag{1}$$

This expression ignores incoherent scattering from the surface of the films but this is expected to be low in sputtered films.

It can be seen that from the plot that the samples with the highest transmittance values are those that were deposited under oxygen flows of 11, 12, and 13sccm. Samples deposited under oxygen flows that were greater or less than this have lower

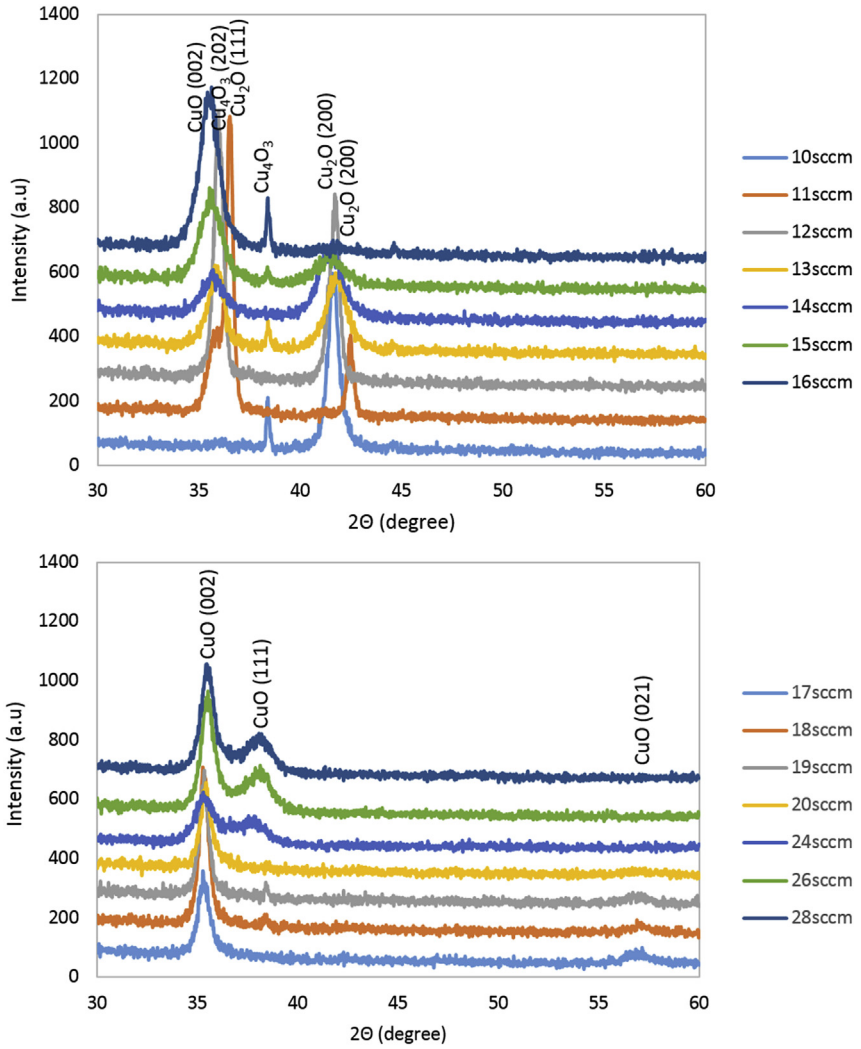

Fig. 2. XRD of samples deposited under various oxygen flows.
Under oxygen flow rates of 10 to 16sccm, all thin film comprise mixed phases of Cu_2O and Cu_4O_3. Under oxygen flow rates of 17scmm or greater, only CuO is present.

transmittance values.

Concentrating on absorptance values in Figs. 4 and 5, it can be seen that the 10sccm sample has the highest absorptance, over the entire range of wavelengths from 400 to 1,100 nm. However, this is consistent with an under-oxidized sample containing some metallic Cu and also, as shown in the XRD, XPS, and Raman results, some Cu_2O. The presence of metallic Cu would render any such thin film not useful for semi-conductor applications, such as a solar cell; however, no other characterisation technique indicated the presence of metallic Cu. From 11 to 13sccm, the films have high absorptance (>0.2) only in the range 400–700 nm and from 15 to 28sccm there is considerable absorptance out to 1,100 nm. It is known from the literature [41] that the extinction coefficient of Cu_2O is lower than that of CuO above 600 nm and so these results are consistent with the increasing oxidation of the films, progressing through Cu_2O, Cu_2O/Cu_4O_3, Cu_4O_3/CuO, and CuO as the oxygen flow rate increases from 11sccm to 28sccm.

Table 1
2θ angles for XRD of plasma-assisted DC sputtered copper oxide films.

Phase	Angle	Reference
CuO (002)	35.4°	JADE5 PDF Table: PDF#48-1548
Cu_4O_3 (202)	35.8°	JADE5 PDF Table: PDF#49-1830
Cu_2O (111)	36.5°	JADE5 PDF Table: PDF#65-3288
Cu_4O_3	38.5°	Blobaum et al., 2003
CuO (111)	38.7°	JADE5 PDF Table: PDF#48-1548
Cu_2O (200)	42.4°	JADE5 PDF Table: PDF#65-3288
CuO (021)	56.7°	JADE5 PDF Table: PDF#48-1548

Although of little practical use in the rather complicated field of nano-structured thin films with variable chemical composition, being only a single number that indicates the onset of optical absorptance, it is nevertheless usual to determine the so-called optical band gap from measurements of transmittance.

The various compositions of Cu_xO_y are known to have various band gap ranges [42]. For Cu_2O it is between 2.20 and 2.90eV [42], for Cu_4O_3 it is between 1.34 and 2.47eV [15], and for CuO it is between 1.21 and 2.20eV [42]. These results are highly variable, varying with the composition, and just as importantly, varying with nano-structure as band gap is known to increase with diminishing grain size. In, for example, solar cell applications, the most important consideration is how absorption varies over the solar spectrum, so the single value of band gap is of little consequence in practice.

The optical band gap, Eg, damping constant, γ, refractive index, n, extinction coefficient, k, and film thicknesses for each sample were calculated by fitting the experimental data with the OJL model

Table 2
Thin film composition at different oxygen flow rates.

O_2 Flow rate (sccm)	Cu_2O (200)	Cu_2O (111)	Cu_4O_3 (202)	CuO (002)	CuO (021)	CuO (111)
10	Present	–	–	–	–	–
11	Present	Present	Present	–	–	–
12	Present	–	Present	–	–	–
13	Present	–	Present	–	–	–
14	Present	–	Present	–	–	–
15	Present	–	Present	–	–	–
16	Present	–	Present	–	–	–
17	–	–	–	Present	Present	–
18	–	–	–	Present	Present	–
19	–	–	–	Present	Present	–
20	–	–	–	Present	–	–
24	–	–	–	Present	–	Present
26	–	–	–	Present	–	Present
28	–	–	–	Present	–	Present

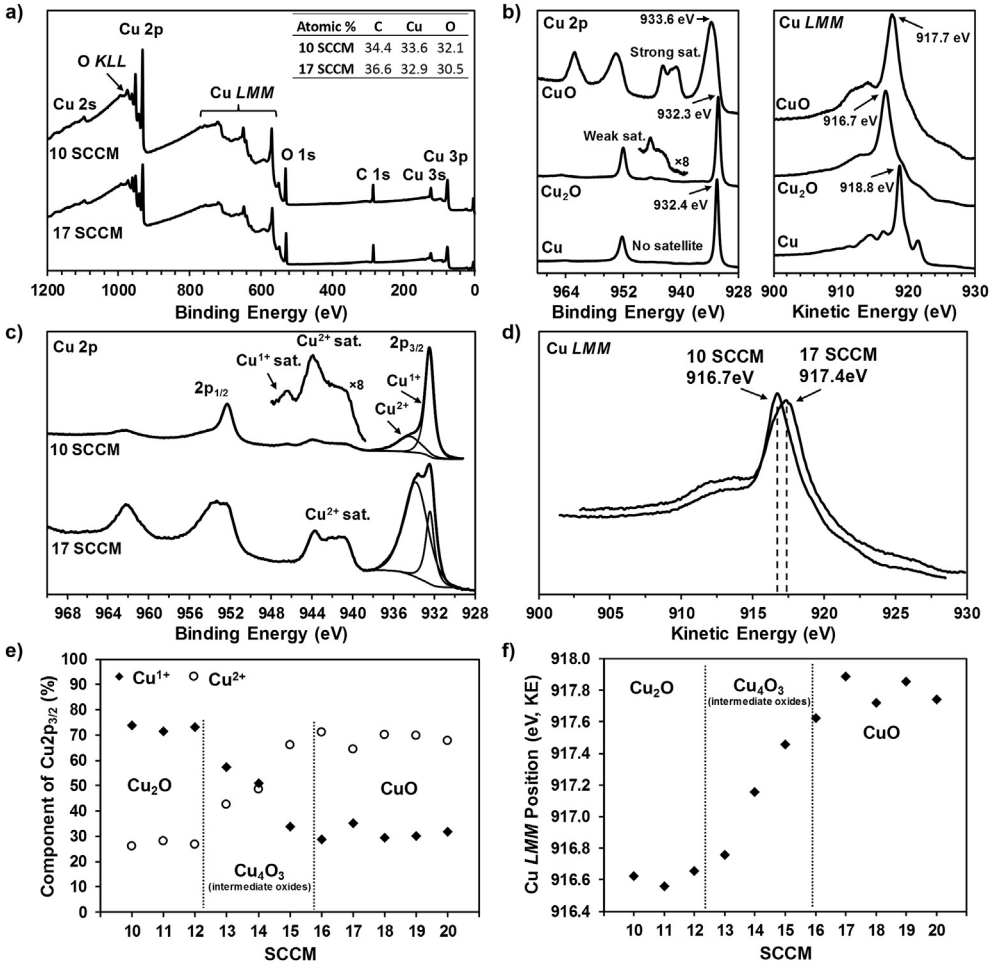

Fig. 3. XPS analysis of the copper surfaces.
(a) XPS Survey spectra from the 10sccm and 17sccm samples showing only the presence of Cu and O signals, with a small carbon contaminant. (b) Reference Cu 2p and Cu LMM spectra for three Cu compositions; Cu metal, Cu_2O and CuO reproduced under CC BY-NC 4.0 [37]. (c) and (d) Cu 2p and Cu LMM spectra for the 10sccm and 17sccm samples. The Cu $2p_{3/2}$ feature can be fitted with one component for each of the Cu^{1+} and Cu^{2+} states. The satellite features observed from 940 to 947eV further substantiate the presence of these states. The Cu LMM peak energy is at 916.7eV for 10sccm and 917.4eV for 17sccm confirming the presence of the Cu^{1+} (Cu_2O) and Cu^{2+} (CuO) states respectively. The relative ratio of the $Cu2p_{3/2}$ components in (c) and the Cu LMM peak energy in (d) is used to monitor the change in oxidation state from Cu^{1+} to Cu^{2+} in (e) and (f) as the flow rate is increased from 10 to 20sccm, with the dominant chemical composition labelled.

using the commercially available SCOUT package from W Theiss Software [43]. Examples of measured and fitted spectra are shown in Fig. 6, with the measured spectrum shown in red and the fitted spectrum shown in blue in each case.

Table 4 shows the derived parameters (at 550 nm wavelength) and the estimated thickness for each film using both software packages. The thicknesses as measured from SEM cross-sections.

The thin films being analysed are nano-structured and

Table 3
Thin film composition at different oxygen flow rates.

O_2 Flow rate (sccm)	Atomic percentage (at.%)			Ratio Cu:O
	Cu	O	C	
10	31.8	30.9	37.3	1:1
11	13.5	18.2	68.3	1:1.3
12	21.2	22.8	56.0	1:1.1
13	28.5	28.8	42.7	1:1
14	29.1	30.2	40.8	1:1
15	31.3	32.1	36.5	1:1
16	31.5	32.9	35.6	1:1
17	30.9	31.4	37.7	1:1
18	30.5	29.7	39.8	1:1
19	30.0	27.4	42.6	1:0.9
20	27.5	23.4	49.1	1:0.9

polycrystalline. In such material, the exponential decay of the valance band's and conduction band's tails need to be considered. The OJL model incorporates a parameter to account for this – damping constant, γ.

The optical band gap values derived by the OJL model for each sample are in accordance with the optical band gap values for the phases determined to be present by XRD, XPS, and Raman. That is, at lower oxygen flows, the presence of Cu_2O and Cu_4O_3 was found to be dominant. The expected band gap values for these phases is 2.2–2.9eV and 1.34–2.47eV, respectively. At higher oxygen flows, the presence of CuO was found to be dominant. The expected band gap value for this phase is 1.21–2.2eV. The optical band gap values

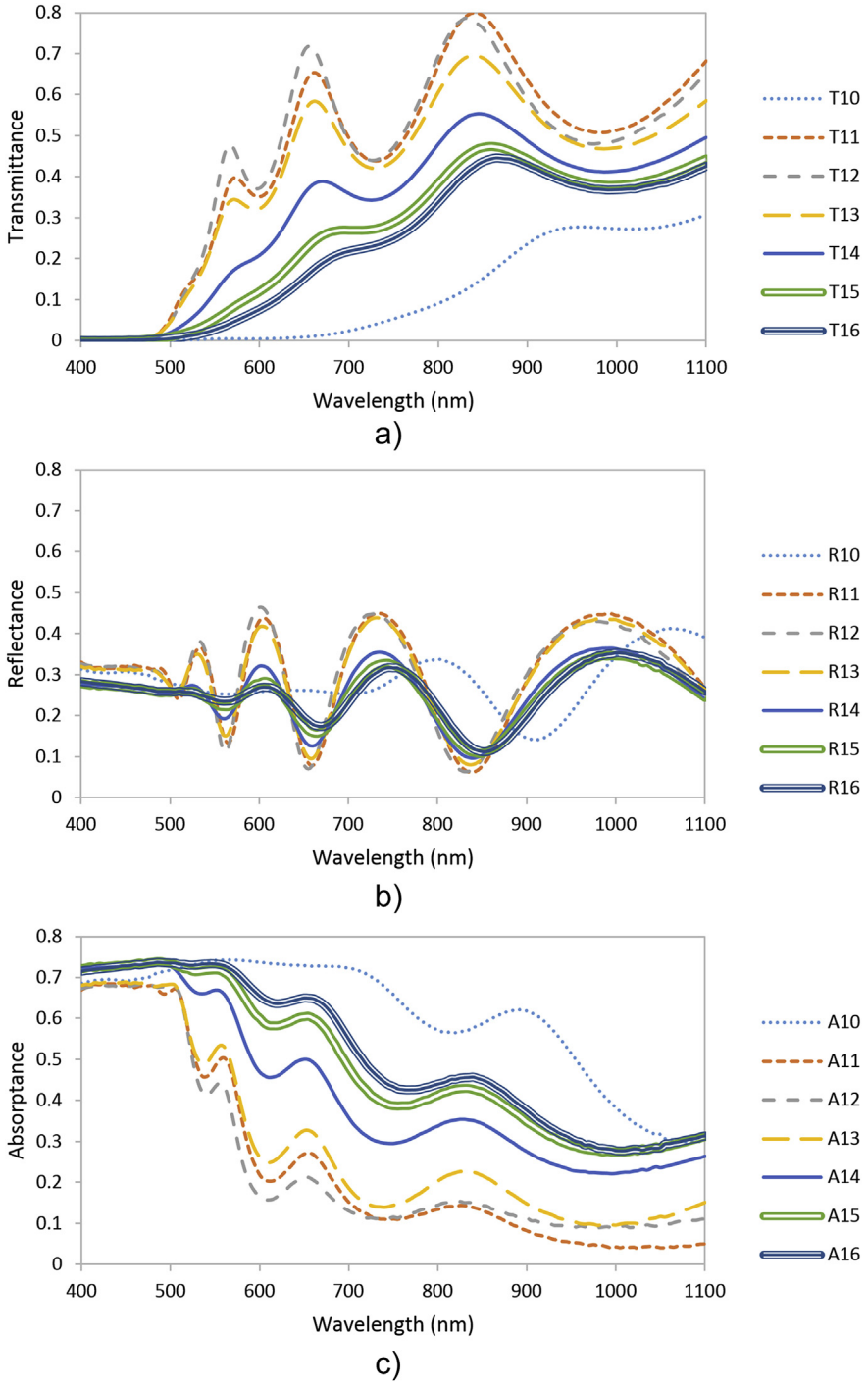

Fig. 4. Optical properties of samples deposited under oxygen flow 10-16sccm.
In general, transmittance decreases and absorptance increases with increased oxygen flow, except for 10sccm which produces a sample with the lowest transmittance and highest absorptance of all samples (10–28sccm).

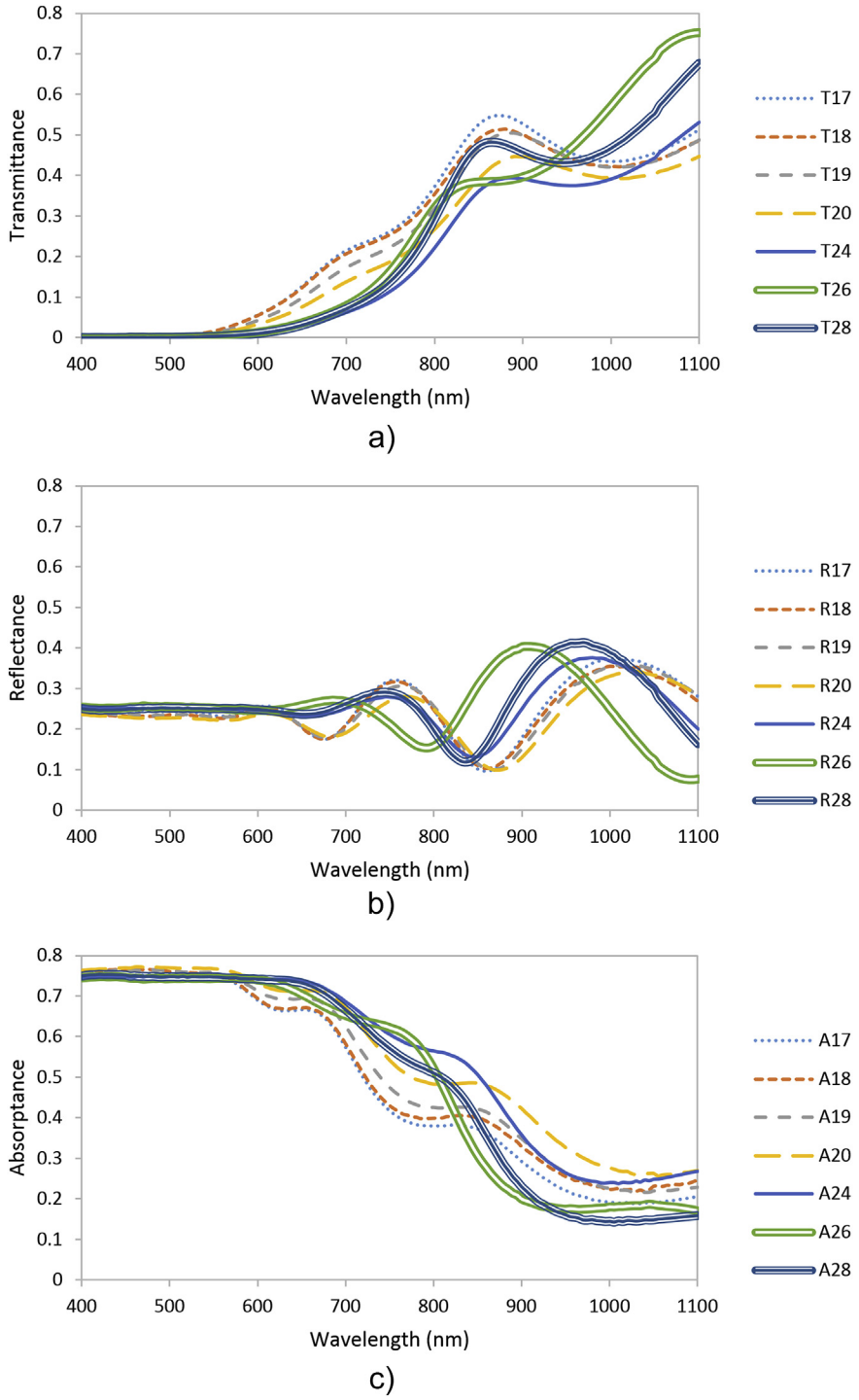

Fig. 5. Optical properties of samples deposited under oxygen flow 17-28sccm.
In general, all the samples have optical properties within a similar band of ± 10%. Transmittance values increase from zero at 600 nm to 50–70% at 1100 nm. Similarly, absorptance values decrease from ~80% at 600 nm to 20–40% at 1100 nm. Below 750 nm, samples deposited under the higher oxygen flows have lower transmittance and higher absorptance values; however, above 750 nm, the ordering becomes more random.

determined by the OJL model appear to track the transition from Cu_2O to CuO being dominant as oxygen flows increase.

Samples produced with an oxygen flow rate of 10sccm are an exception to this trend; however, as mentioned previously, this sample contains some Cu metal and so the spectra cannot be fitted by the OJL model.

Similarly, the OJL model confirms that the extinction coefficient of Cu_2O dominant films is lower than that of CuO dominant films, as expected. However, the extinction coefficient of the 10sccm sample is anomalously high; again, this is likely due to the presence of metal Cu.

The thicknesses derived by OJL model and SEM are broadly in agreement with each other.

4.5. Raman measurements

Initial Raman measurements showed that samples grown in the MARS system formed Cu_2O as well as Cu_4O_3 in higher O_2 processed samples. The Raman results are shown in Fig. 7 for oxygen flows of 10 to 28sccm. By comparison with Table 5, which notes the various copper oxide Raman Shift values, it can be seen that at 10sccm, Cu_2O is the only phase present; between 11sccm and 16sccm, mixed phases of Cu_2O and Cu_4O_3 are present; between 17sccm and 20sccm, Cu_4O_3 is the only phase present; at 24sccm, mixed phases of Cu_4O_3 and CuO are present; and at 26sccm and greater, CuO is the only phase present.

The presence of the various forms of copper oxide are summarised in Table 6.

It can be noted that there are differences between the XRD results and Raman results for the 17sccm to 24sccm samples. For 17sccm to 20sccm, XRD detects the presence of CuO, whereas Raman detects the presence of Cu_4O_3. For 24sccm, XRD detects the presence of CuO, whereas Raman detects the presence of a mixture Cu_4O_3 and CuO. However, the XRD and Raman techniques probe fundamentally different physical properties. XRD derives information from crystal plains and is therefore sensitive to the crystallinity of the sample, whereas Raman is sensitive to the polarizability of molecular bonds, which can identify amorphous phases more so than XRD. Therefore, in mixtures where different crystal orientations will affect XRD intensity, Raman will be able to identify different phases where XRD does not, ie, in the 24sccm sample. Thus, XRD can determine structural information of the bulk of the film, whereas Raman measurements provide information of the film surface (that may be of different composition to the bulk) as noted in other research that "Raman spectroscopy, unlike XRD, can only get the structure information from the top layer of the thin film" [45].

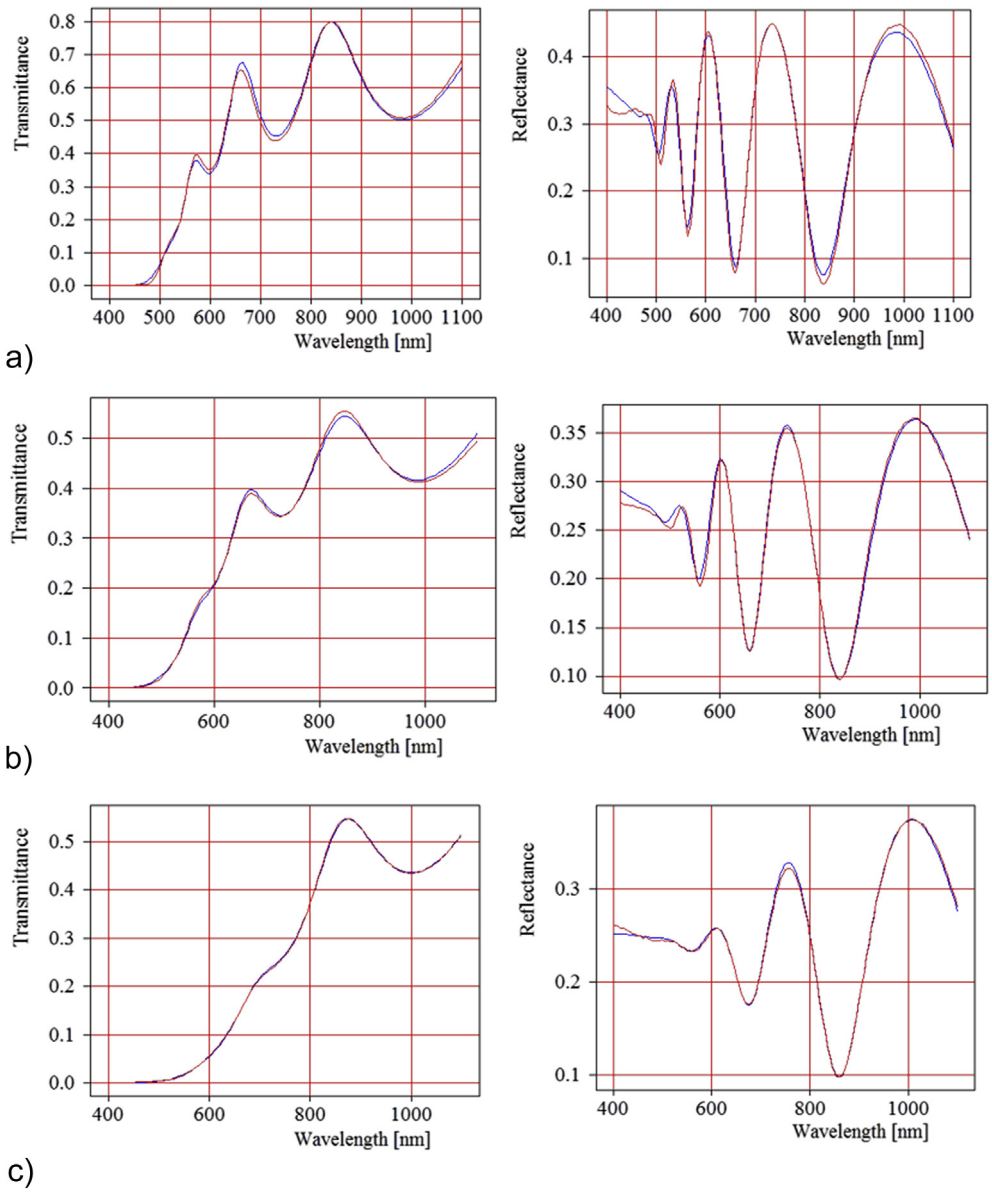

Fig. 6. Example simulated optical spectra by OJL model.
Measured spectra are shown in red and fitted spectra are shown in blue. (For interpretation of the references to colour in this figure legend, the reader is referred to the web version of this article.)

Table 4
Optical properties simulation parameters with SEM thickness data.

O_2 Flow (sccm)	SCOUT-OJL					SEM
	Eg (eV)	γ (eV)	n	k	Thickness (nm)	Thickness (nm)
10	1.01	0.30	3.10	0.53	462	454
11	2.22	0.15	3.08	0.08	462	487
12	2.19	0.09	3.16	0.07	448	449
13	2.23	0.13	3.07	0.09	460	486
14	1.94	0.15	3.08	0.18	470	458
15	1.44	0.02	2.56	0.21	477	479
16	1.31	0.02	2.92	0.27	474	481
17	1.29	0.03	2.92	0.30	482	479
18	1.31	0.04	2.78	0.32	488	502
19	1.23	0.01	2.79	0.36	478	477
20	1.23	0.07	2.73	0.38	500	511
24	1.22	0.05	2.85	0.62	453	430
26	1.25	0.06	2.86	0.67	412	420
28	1.28	0.06	2.86	0.67	443	438

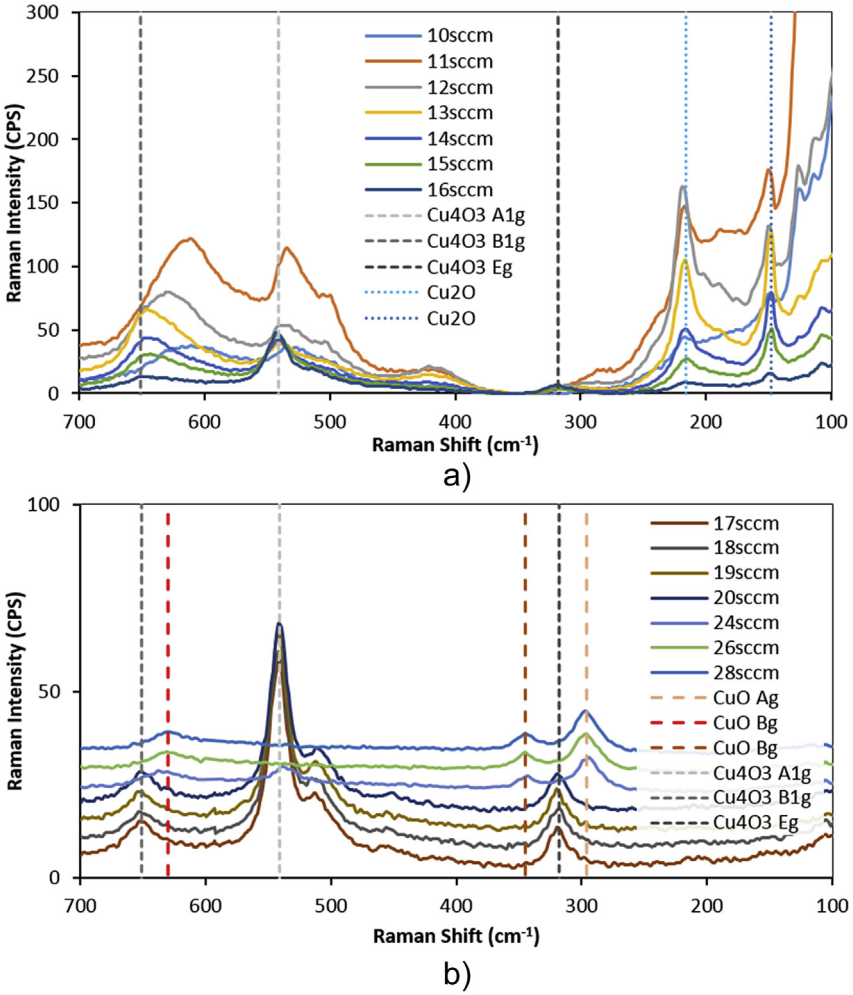

Fig. 7. Raman measurements of MARS thin films at various oxygen flows.
The peaks indicate the presence of Cu_2O for thin films produced under oxygen flows between 10sccm and 16sccm, the presence of Cu_4O_3 under oxygen flows between 11sccm and 24sccm, and the presence of CuO under oxygen flows between 24sccm and 28sccm.

5. Conclusions

It is demonstrated that the sputtered films develop through CuO, Cu_4O_3 and Cu_2O mixed phases as oxygen flow rate is increased and can be successfully and reproducibly grown at room temperature. A pure form of Cu_2O is only produced under an oxygen flow rate of 10sccm; however, this may be contaminated by Cu metal.

The results indicate that Cu_4O_3 can be reliably produced by MARS at oxygen flow rates between 11sccm and 16sccm, and

Table 5
Raman shifts of Cu_xO_y [15,44].

Raman shift (cm^{-1})	Copper oxide phase
148	Cu_2O
216	Cu_2O
296	CuO Ag
318	Cu_4O_3 Eg
345	CuO Bg
541	Cu_4O_3 A1g
651	Cu_4O_3 B1g

Table 6
Interpretation of copper oxide content based on Raman observations.

O_2 Flow rate (sccm)	Cu_2O	Cu_4O_3	CuO
10	Present	–	–
11	Present	Present	–
12	Present	Present	–
13	Present	Present	–
14	Present	Present	–
15	Present	Present	–
16	Present	Present	–
17	–	Present	–
18	–	Present	–
19	–	Present	–
20	–	Present	–
24	–	Present	Present
26	–	–	Present
28	–	–	Present

possibly at higher oxygen flow rates as well.

For the production of solar cells, Cu_2O thin films are preferable due to the better optical and electrical properties over the other phases of copper oxide.

It is concluded that careful control of the oxygen flow rate (and therefore partial pressure of oxygen) is critically important in the production of particular stoichiometries of copper oxides. It has also been shown that detailed characterisation of the sputtered films is possible with the aid of XPS, XRD, optical and Raman measurements. The OJL model was used to determine the E gap and optical properties and confirmed by the other methods. In particular, given that many of the earlier papers to be found in the literature ignored the possibility of the formation of Cu_4O_3, their findings will possibly require some reconsideration.

Acknowledgments

XPS data were acquired at the National EPSRC XPS User's Service at Newcastle University, an EPSRC Mid-Range Facility. This work incorporates data from the Victorian node of the Australian National Fabrication Facility (ANFF), a company established under the National Collaborative Research Infrastructure Strategy to provide nano and microfabrication facilities for researchers in Australia, through the La Trobe University Centre for Materials and Surface Science. Data are reproduced under a Creative Commons licence (CC BY-NC 4.0 International).

References

[1] S.S. Jeong, A. Mittiga, E. Salza, A. Masci, S. Passerini, Electrodeposited ZnO/Cu_2O heterojunction solar cells, Electrochimica Acta 53 (2008) 2226–2231.
[2] F. Li, R. Waddingham, W. Milne, A. Flewitt, S. Speakman, Low temperature (<100 °C) deposited P-type cuprous oxide thin films: Importance, Thin Solid Films 520 (2011) 1278–1284.
[3] A. Parretta, M.K. Jayaraj, A. Di Nocera, S. Loreti, L. Quercia, A. Agati, Electrical and optical properties of copper oxide films prepared by reactive RF magnetron sputtering, Phys. Status Solida A 155 (1996) 399–404.
[4] F. Oba, F. Ernst, Y. Yu, R. Liu, H.M. Kothari, J.A. Switxer, Epitaxial growth of cuprous oxide electrodeposited onto semiconductor and metal substrates, J. Am. Ceram. Soc. 88 (2) (2005) 253–270.
[5] K. Akimoto, S. Ishizuka, M. Yanagita, Y. Nawa, G.K. Paul, T. Sakurai, Thin film deposition of Cu_2O and application for solar cells, Sol. Energ. 80 (6) (2006) 715–722.
[6] P.J.M. Isherwood, Copper zinc oxide: investigation into a p-type mixed metal oxide system, Vacuum 139 (2017) 173–177.
[7] T.J. Richardson, J.L. Slack, M.D. Rubin, Electrochromism of copper oxide thin films, in: Presented at 4th International Meeting on Electrochromism, 2000. Uppsala, Sweden.
[8] B. Balamurugan, B.R. Mehta, Optical and structural properties of nanocrystalline copper oxide thin films prepared by activated reactive evaporation, Thin solid films 96 (1) (2001) 90–96.
[9] A.A. Ogwu, E. Bouquerel, O. Ademosu, S. Moh, E. Crossan, F. Placido, The influence of RF power and oxygen flow rate during deposition on the optical transmittance of copper oxide thin films prepared by reactive magnetron sputtering, J. Phys. D Appl. Phys. 38 (2005a) 266–271.
[10] V.F. Drobny, D.L. Pulfrey, Properties of reactively-sputtered copper oxide thin films, Thin Solid Films 61 (1979) 89–98.
[11] K.J. Blobaum, D. Van Heerden, A.J. Wagner, D.H. Fairbrother, T.P. Weihs, Sputter-deposition and characterization of paramelaconite, J. Mater. Res. 18 (7) (2003) 1535–1542.
[12] J.F. Pierson, A. Thobor-Keck, A. Billard, Cuprite, paramelaconite and tenorite films deposited by reactive magnetron sputtering, Appl. Surf. Sci. 210 (3–4) (2003) 359–367.
[13] J. Medina-Valtierra, C. Frausto-Reyes, G. Camarillo-Martínez, J.A. Ramírez-Ortiz, Complete oxidation of isopropanol over Cu_4O_3 (paramelaconite) coating deposited on fiberglass by CVD, Appl. Catal. A General 356 (1) (2009) 36–42.
[14] D. Reppin, A. Polity, B.K. Meyer, S. Shokhovets, Optical and electrical properties of Cu_2O, Cu_4O_3 and CuO, in: MRS Proceedings, vol. 1494, Cambridge University Press, 2013, pp. 165–169.
[15] A.S. Zoolfakar, R.A. Rani, A.J. Morfa, A.P. O'Mullane, K. Kalantar-Zadeh, Nanostructured copper oxide semiconductors: a prespective on materials, synthesis methods and applications, J. Mater. Chem. C 2 (27) (2014) 5247–5270.
[16] A.A. Ogwu, T.H. Darma, E. Bouquerel, Electrical resistivity of copper oxide thin films prepared by reactive magnetron sputtering, J. Achiev. Mater. Manuf. Eng. 24 (1) (2007) 172–177.
[17] B.C. Castle, Memristive Properties of Thin Film Cuprous Oxide, MSc thesis, Air University, Wright-Patterson Air Force Base, Ohio, 2011.
[18] L. Chua, Linear transformation converter and its application to the synthesis of nonlinear networks, IEEE Trans. Circ. Theor. 17 (4) (1970) 584–594.
[19] K. Fujimoto, T. Oku, T. Akiyama, A. Suzuki, Fabrication and characterization of copper oxide-zinc oxide solar cells prepared by electrodeposition, J. Phys. Conf. Ser. 433 (1) (2013) 12–24.
[20] T.K.S. Wong, S. Zhuk, S. Masudy-Panah, G.K. Dalapati, Current status and future prospects of copper oxide heterojunction solar cells, Materials 9 (4) (2016) 271.
[21] J.J. Loferski, Theoretical considerations governing the choice of the optimum semiconductor for photovoltaic solar energy conversion, J. Appl. Phys. 27 (7) (1956) 777–784.
[22] L.C. Olsen, R.C. Bohara, M.W. Urie, Explanation for low-efficiency Cu2O Schottky-barrier solar cells, Appl. Phys. Lett. 34 (1) (1979) 47.
[23] T. Minami, Y. Nishi, T. Miyata, Heterojunction solar cell with 6% efficiency based on an n-type aluminum–gallium–oxide thin film and p-type sodium-doped Cu_2O sheet, Appl. Phys. Express 8 (2) (2015).
[24] K. Ozawa, Y. Oba, K. Edamota, Formation and characterization of the Cu_2O overlayer on Zn(0001), J. Sci. 603 (13) (2009) 2163–2170.
[25] A.A. Ogwu, E. Bouquerel, O. Ademosu, S. Moh, E. Crossan, F. Placido, An investigation of the surface energy and optical transmittance of copper oxide thin films by reactive magnetron sputtering, Acta Mater. 53 (2005b) 5151–5159.
[26] S.C. Ray, Preparation of copper oxide thin film by the sol–gel-like dip technique and study of their structural and optical properties, Sol. Energy Mater. Sol. cells 68 (2001) 307–312.
[27] G.N. Papadimitropoulos, N. Vourdas, E. Vamvakas, D. Davazoglou, Optical and structural properties of copper oxide thin films grown by oxidation of metal layers, Thin Solid Films 515 (2006) 2428–2432.
[28] R. Kita, T. Hase, R. Itti, M. Sasaki, T. Morishita, S. Tanaka, Synthesis of cupric oxide films using mass-separated low-energy beam, Appl. Phys. Lett. 60 (1992) 2624–2630.
[29] F.K. Mugwang, P.K. Karimi, P.K. Njoroge, O. Omayio, S.M. Waita, Optical characterisation of copper oxide films prepared by reactive DC magnetron sputtering for solar cell applications, Int. J. Thin Films Sci. Technol. 2 (1) (2013) 15–24.
[30] S. Moh, Microwave Assisted Sputtered Coatings, PhD Thesis, University of the West of Scotland, Paisley, Scotland, UK, 2012.
[31] Y. Alajlani, F. Placido, D. Gibson, H.M. Chu, S. Song, L. Porteous, S. Moh, Nanostructured ZnO films prepared by hydro-thermal chemical deposition and microwave-activated reactive sputtering, in: 57th Annual Technical Conference Proceedings, 2015. Santa Clara, CA.
[32] M. Mazur, D. Wojcieszak, J. Domaradzki, D. Kaczmarek, S. Song, F. Placido, TiO2/SiO2 multilayer as an antireflective and protective coating deposited, Opto Electron. Rev. 21 (2) (2013) 233–238.
[33] Z. Gou, F. Placido, Aluminum oxynitride rugate filters grown by reactive rf sputtering, Proc. SPIE 4086 (2000) 791–794.

[34] F. Placido, Z. Gou, C. Rebecchi, Microwave-assisted reactive sputtering of aluminum oxynitrides, Proc. SPIE 4086 (2000) 376–381.
[35] P.J. Kelly, R.D. Arnell, Magnetron sputtering: a review of recent developments and applications, Vacuum 56 (3) (2000) 159–172.
[36] S.K. O'Leary, S.R. Johnson, P.K. Lim, The relationship between the distribution of electronic states and the optical absorption spectrum of an amorphous semiconductor: an empirical analysis, J. Appl. Phys. 82 (7) (1997) 3334–3340.
[37] A.J. Barlow, A.J. McDonald, P.J. Pigram, R.T. Jones, XPSSurfA – an online collaborative surface analysis data reproduced under creative Commons attribution non commercial 4.0 international, Full terms at: https://creativecommons.org/licenses/by-nc/4.0/, 2017. (Accessed 10 July 2017) https://cmsshub.latrobe.edu.au/xpsdatabase [Online]. Available:.
[38] J.P. Espinos, J. Morales, A. Barranco, A. Caballero, J.P. Holgado, A.R. Gonzalez-Elipe, Interface effects for Cu, CuO, and Cu_2O deposited on SiO_2 and ZrO_2. XPS determination of the valence state of copper in Cu/SiO_2 and Cu/ZrO_2 catalysts, J. Phys. Chem. B 106 (27) (2002) 6921–6929.
[39] I. Platzman, R. Brener, H. Haick, R. Tannenbaum, Oxidation of polycrystalline copper thin films at ambient conditions, J. Phys. Chem. C 112 (4) (2008) 1101–1108.
[40] M.C. Biesinger, Advanced analysis of copper X-ray photoelectron spectra, Surf. Interface Anal. (2017), http://dx.doi.org/10.1002/sia.6239. Early View (Online).
[41] C.G. Ribbing, A. Roos, Part II: critiques, subpart 3: insulators, copper oxides (Cu_2O, CuO), in: E.D. Palik (Ed.), Handbook of Optical Constants of Solids II, Academic Press, London, UK, 1997, pp. 875–882.
[42] F.K. Mugwang'a, P.K. Karimi, W.K. Njoroge, O. Omayio, S.M. Waita, "Optical characterization of copper oxide thin films prepared by reactive dc magnetron sputtering for solar cell applications, Int. J. Thin Films Sci. Technol. 2 (1) (2013) 15–24.
[43] W. Theiss, OJL interband transition model for amorphous materials - a brief tutorial [Online]. Available: http://www.mtheiss.com/ojlmodel.htm. (Accessed 13 February 2017).
[44] L. Debbichi, M.C. Marco, D. Lucas, F.J. Pierson, P. Krüger, Vibrational properties of CuO and Cu_4O_3 from first-principles calculations, and raman and infrared spectroscopy, J. Phys. Chem. C 116 (2012) 10232–10237.
[45] Y.S. Gong, C. Lee, C.K. Yang, Atomic force microscopy and Raman spectroscopy studies on the oxidation of Cu, J. Appl. Phys. 77 (1995) 5422.